JACS
JOURNAL OF THE AMERICAN CHEMICAL SOCIETY

Chiral Arrangement of Achiral Au Nanoparticles by Supramolecular Assembly of Helical Nanofiber Templates

Sung Ho Jung,[†] Jiwon Jeon,[‡] Hyungjun Kim,[*,‡] Justyn Jaworski,[*,∥,⊥] and Jong Hwa Jung[*,†]

[†]Department of Chemistry and Research Institute of Natural Sciences, Gyeongsang National University, Jinju 660-701 Korea

[‡]Graduate School of Energy, Environment, Water, and Sustainability, Korea Advanced Institute of Science and Technology, Daejeon 305-701 Korea

[∥]Department of Chemical Engineering, Hanyang University, Seoul 133-791 Korea

[⊥]Institute of Nano Science and Technology, Seoul 133-791 Korea

Ⓢ *Supporting Information*

ABSTRACT: Chiral materials composed of organized nanoparticle superstructures have promising applications to photonics and sensing. Reliable customization of the chiroptical properties of these materials remains an important goal; hence, we report a customizable scheme making use of modular gelator components for controlling the helicity and formation of nanofibers over long length scales resulting in hydrogel templates. Controlled growth of gold nanoparticles at spatially arranged locations along the nanofiber is achieved by UV reduction of Au(I) ions on the supramolecular templates. The resulting materials were found to have significant interparticle interactions and well-defined helicity to provide high quality, chiroptically active materials. With this novel approach, the tailored assembly of nanoparticle superstructures with predictable chiroptical properties can be realized in high yield, which we expect to allow rapid advancement of chiral nanomaterials research.
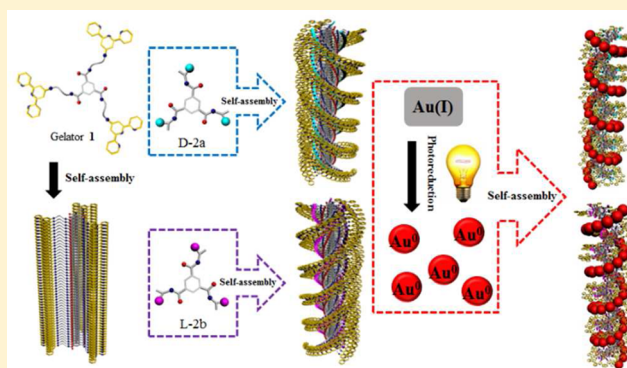
INTRODUCTION

Tuning the spatial arrangement of nanoparticle building blocks within hybrid materials can offer a means for controlling specific material properties. A number of reviews have explored the diversity of complex structures that have been formed with nanoparticle assemblies,[1] many of which show unique and interesting optical properties.[2] While the literature is replete with accounts of controlled spatial assembly of nanoparticles,[3] more recently, the template-driven assembly of 3D chiral architectures of nanoparticles has become an especially active area of research. Successful endeavors utilizing biopolymeric templates including DNA,[4] peptides,[5] and lipids[6] have revealed the coiled formation of nanoparticles and even nanorods[7] assembled into helical bundles. The use of chiral templates for nanoparticle assembly is particularly innovative and was first demonstrated utilizing Ag nanoparticles synthesized into chiral arrangements using a DNA helical template yielding an optically active material.[8] Related research has shown the use of amphiphilic peptide-based nanoribbons allowing stereochemical arrangement of gold nanoparticles on the surface,[5a,9] which has demonstrated the feasibility of rationally designing templates for "bottom-up" fabrication of nanoparticle superstructures. In more recent works, the use of mesoporous silica[10] and even coordinatable organogelator components of a sol−gel system[11] have also proved to be effective approaches for the formation of nanoparticle superstructures.

The ability to design and create materials with control over the size as well as the spatial organization of nanoparticles remains an important objective of this field. Obtaining a system that offers customizability in altering or enhancing the chiroptical properties of the material will find many practical applications and will be of value in improving our level of understanding of these collective chiroptical properties. A recent review has noted the stringent requirements of having well-defined helicity and sufficient interparticle interactions of chiral NP assemblies in order to obtain such optical activity enhancement.[12] As a step toward the ultimate goal of creating tailored systems with high optical activity, we have explored the development of a modular method for the "bottom up" assembly of organized nanoparticle superstructures having controlled size on well-defined helical nanofiber templates.

To advance this area of research, we hereby provide a new method for achieving the growth of organized nanoparticles with tunable sizes and well-defined helical order. Our modular approach utilizes a gelator template moiety in combination with
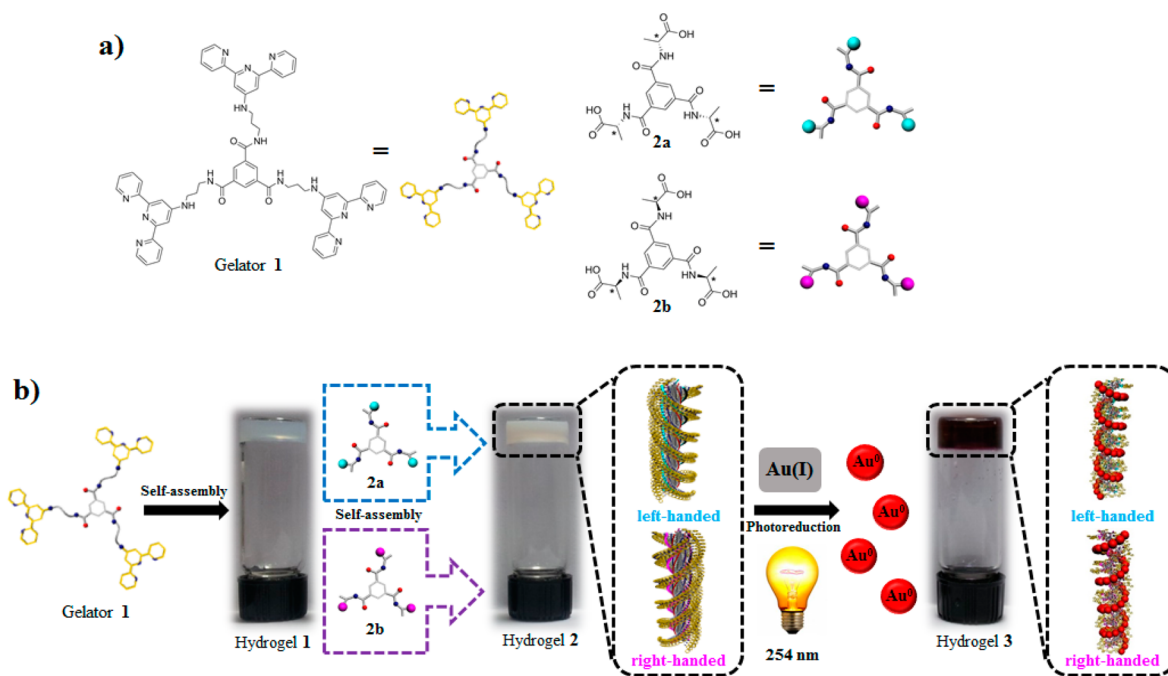
Figure 1. (a) Chemical structures of gelator **1** and chiral components **2a** (D-form) and **2b** (L-form). (b) Overview of hydrogel formation resulting from controlled assembly of nanofibers with tunable helicity by addition of chiral **2a** or **2b** components, and further addition of Au(I) followed by UV exposure to generate helically templated gold nanoparticle superstructures.

specific helicity-directing molecular components. UV reduction of Au(I) ions is utilized to afford organized gold nanoparticles. Specifically, we demonstrate the formation of left-handed as well as right-handed helical gold nanoparticle assemblies with customizable sizes from as small as 2 nm up to 200 nm. Helical nanofiber templates, capable of hydrogel formation, were created over long length scales, and subsequent formation of nanoparticle superstructures on the templates offered control over the surface plasmon absorption wavelengths. The helically arranged nanoparticles were highly correlated with respect to position, as the nanoparticle organization allowed significant enhancement of the material's chiroptical properties. In this work, we provide a detailed characterization of our customizable gelator template system for the formation of hierarchically assembled materials with tunable chiroptical activity, and we offer a discussion of the prospective design principles for modifying such material properties.

An overview of our design strategy used to generate helical nanoparticle superstructures first entailed the self-assembly of nanofibers, prepared as shown in Figure 1 and Scheme S1, in which gelator **1** is dissolved in a mixture of DMSO and water. By utilizing gelator molecules along with novel chiral components (**2a** or **2b**, Scheme S2) with directing stereochemistries, we could yield hydrogels composed of nanofibers having controlled helicity. Through $\pi-\pi$ stacking of the chiral molecules with the gelator, we could induce helicity in the self-assembled nanofibers. We show that the addition of L- or D-form chiral components can initiate the formation of either right- or left-handed nanofibers, respectively, with varying levels of optical activity depending on the molar composition as confirmed by circular dichroism (CD) spectroscopy. From detailed characterization and quantum mechanical density functional theory (DFT) calculations, we identified the atomistic origin of the distinct structural arrangements of nanofibers assembled from single as well as dual component mixtures. Further results with the well-defined helical nano-

fibers of gel **1/2a** or **1/2b** revealed that the exposed anionic carboxylate groups served as templates for Au(I) ions thereby allowing the controlled spatial arrangement of gold nanoparticles on the surface of the helical nanofibers formed after UV reduction by photoirradiation. Tuning the amount of Au(I) ion and the extent of UV irradiation provided a reliable means for adjusting the absorption wavelength of the chiroptical material through control over the nanoparticle size within the helically organized superstructures.

■ METHODS

Characterization. ^{1}H and ^{13}C NMR spectra were measured on a Bruker DRX 300 apparatus. IR spectra were obtained for KBr pellets, over the range of 400−4000 cm^{-1}, with a Shimadzu FT-IR 8400S instrument, and mass spectra were obtained by a JEOL JMS-700 mass spectrometer.

N-([2,2′:6′,2″-terpyridin]-4′-yl)propane-1,3-diamine (**4**). 4′-Chloro-[2,2′;6′,2″]terpyridine (4′-chloroter-pyridine), (0.9 g, 3.36 mmol) was suspended in 1,3-diamino propane (6.5 mL). Upon heating a yellow solution was observed. The reaction mixture was then heated under reflux conditions (120 °C) overnight. After cooling to room temperature, H$_2$O (50 mL) was added, and a white precipitate was formed, which was filtered and further washed with H$_2$O. The solid was dissolved in dichloromethane and extracted twice with H$_2$O. The organic layers were combined, dried over Na$_2$SO$_4$, and filtered and the solvent removed under reduced pressure to yield a white solid (0.8 g, 78%). mp 147 °C; ^{1}H NMR (300 MHz, CDCl$_3$) 8.67 (d, 2H, CH6 + 6″, *J* = 4.8 Hz) 8.62 (d, 2H, CH3 + 3″, *J* = 7.8 Hz) 7.83 (t, 2H, CH4 + 4″, *J* = 7.8, 7.8 Hz) 7.66 (s, 2H, CH3′ + 5′), 7.31 (t, 2H, CH5 + 5″, *J* = 6.0, 6.3 Hz), 5.16 (t, 1H, NH, *J* = 4.5, 5.0 Hz), 3.47 (m, 2H, NHCH$_2$), 2.91 (t, 2H, CH$_2$, *J* = 6.6, 6.3 Hz) 1.83 (m, 2H, NH$_2$CH$_2$) 1.25 (bs, 2H, NH$_2$); ^{13}C NMR (125 MHz, CDCl$_3$) 156.89, 155.84, 155.49, 148.82, 136.66, 123.41, 121.32, 104.62, 41.68, 40.42, 32.33; IR(KBr, cm^{-1}): 3353, 3245, 3126, 3051, 3012, 2932, 2852, 1618, 1572, 1564, 1515, 1464, 1456, 1447, 1407, 1355, 1339, 1314, 1296, 1225, 1113, 1091,1069, 1040, 986, 924, 861, 798, 743, 697, 657; ESI-MS: *m/z* 306.25 [M + H]$^+$; Calculated for C$_{18}$H$_{19}$N$_5$ [M + H]$^+$ 306.3734; found 306.3728.

6447

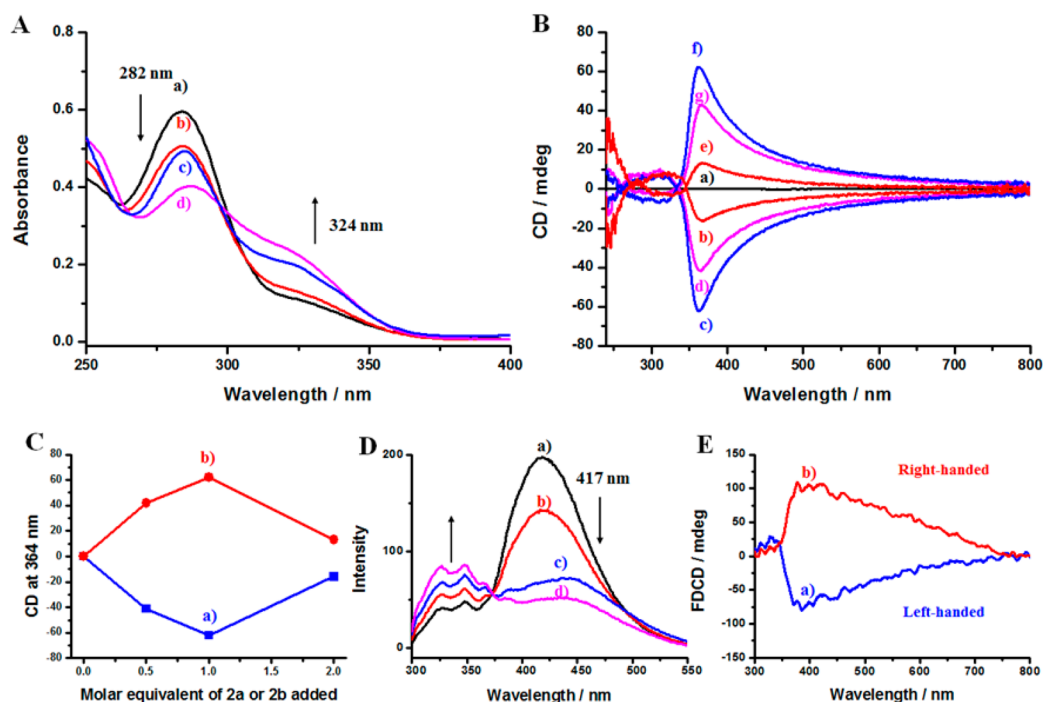dx.doi.org/10.1021/ja5018199 | *J. Am. Chem. Soc.* 2014, 136, 6446−6452

Figure 2. (A) UV−vis spectra of hydrogel **1** without (a) **2a** and with (b) 0.5 equiv, (c) 1.0 equiv, and (d) 2.0 equiv of **2a** in DMSO/water. (B) CD spectra of hydrogel **1** having (a) 0 equiv, (b) 0.5 equiv., (c) 1.0 equiv, and (d) 2.0 equiv of **2a**(D-form) or **2b** (L-form) in DMSO/water. (C) Comparison of the CD spectra maxima at 364 nm revealing relative enhancement when using various molar equivalents of **2a** (blue line) or **2b** (red line) added to gelator **1**. (D) Fluorescence emission spectra of hydrogel **1** without (a) **2a** and with (b) 0.5 equiv, (c) 1.0 equiv, and (d) 2.0 equiv of **2a** in DMSO/water. (E) FDCD spectra of (a) hydrogel **1** with **2a** (1.0 equiv) and (b) hydrogel **1** with **2b** (1.0 equiv) in DMSO/water.

Benzene-1,3,5-tricarboxylic Acid Tris([3-([2,2′;6′,2″]-terpyridin-4′-ylamino)-propyl]-amide) (1, gelator 1). The gelator **1** was prepared according to a literature procedure.[13] A solution of **4** (0.05 g, 0.164 mmol) in dichloromethane was allowed to cool in an acetone/ice bath for 15 min before adding 1,3,5-benzenetricarbonyl trichloride (0.014 g, 0.053 mmol). A white precipitate was observed, and the reaction mixture was further stirred at room temperature overnight. The solid was then filtered and washed with dichloromethane to yield a beige solid (0.051 g, 90%). mp 230 °C; ^{1}H NMR (300 MHz, CD_3OD) 8.74 (s, 1H, CH_tpy), 8.72 (s, 1H, CH_tpy), 8.64 (s,1H,CH_benzene), 8.25 (s, 1H, CH_tpy), 8.14−8.00 (3H, CH_tpy), 7.64−7.47 (4H, CH_tpy), 3.65 (m, 2H, CH_2), 3.65 (m, 2H, CH_2), 2.11 (m, 2H, CH_2); ^{13}C NMR (125 MHz, CD_3OD) 167.22, 160.36, 160.04, 149.99, 146.83, 145.90, 138.54, 138.25, 135.17, 131.91,131.67, 131.17, 129.31, 126.85, 121.73, 121.73,110.65, 106.05, 100.79, 41.30, 37.43, 28.21; IR(KBr, cm^{-1}): 3245, 3094, 3058, 2942, 2871,1637, 1589, 1527, 1464, 1443, 1352, 1297, 1270, 1238, 1159, 1124, 1090, 1034, 993, 908, 867, 785, 736; ESI-MS: m/z 358.25 [M + 3H]$^{3+}$/3, 536.92 [M + 2H]$^{2+}$/2, 1072.58 [M + H]$^+$; Calculated for C_{63}H_{59}N_{15}O_3 1073.4925; found 1073.4930.

Compounds 2a and 2b. Trimesoyltri(D-alanine) (**2a**) and trimesoyltri(L-alanine) (**2b**) were prepared according to a literature procedure.[14] A water solution (30 mL) of D- or L-alanine (5.400 g, 0.02 mol) and NaOH (2.400 g, 0.06 mol) was also prepared. The freshly prepared 1,3,5-benzenetricarbonyl trichloride and alanine solution were alternatively added slowly in small portions into a round-bottomed flask in an ice-bath, together with the addition of a 4 mol L^{-1} NaOH solution to adjust the pH value to 8.0−9.0. This procedure was finished in an hour. The resulting solution was stirred for another 3 h and then acidified by the addition of a concentrated HCl solution to adjust the pH value at 1−2. Further cooling of the resulting mixture in an ice-bath for several minutes gave a white precipitate, which was separated by filtration and washed by cold water. The crude product was further washed with a 1:1 ethanol and water solution (30 mL), giving a pure product in a yield of 80% after filtration and dryness. m.p.: 216−218 °C; ^{1}H NMR (300 MHz, D_2O) 8.13 (s, 3H, Ar−H), 4.45 (q, 3H, 3J = 7.2 Hz, −CH(CH3)COO), 1.39 (d, 9H, 3J = 7.2 Hz,

−CH3); ^{13}C NMR (125 MHz, D_2O) 176.4, 167.9, 133.8, 129.4, 49.4, 15.9. IR (KBr, cm^{-1}): 3366, 3220, 3015, 1727, 1623, 1589, 1535, 1460, 1335, 1309, 1212, 1169, 1118, 912, 807; ESI-MS: m/z 422.00 [M$^+$]; Calculated for C_{18}H_{21}N_3O_9 [M$^+$] 423.1278; found 423.1254.

Chloro(tetrahydrothiophene) gold(I). Chloro(tetrahydrothiophene) gold(I) was prepared according to existing literature procedures (Scheme S3).[15] Tetrahydrothiophene (0.19 mL, 2.1 mmol) was added dropwise to a solution of HAuCl_4·3H_2O (394 mg, 1 mmol) in a mixture of water (0.7 mL) and ethanol (3.3 mL). The reaction mixture was stirred for 30 min at room temperature until the yellow precipitate was transformed to a white solid. The resulting white precipitate was filtered, washed with ethanol, and vacuum dried. Yield 95%.

Preparation of Supramolecular Gels. In a typical gelation study experiment, a solution of **2a** or **2b** [200 μL, 0.5−2.0 equiv] in water was added to solution of gelator **1** [1.0 wt % in DMSO] in a vial. Each mixture was heated to 60−70 °C and bath sonicated for 3 min to get a homogeneous solution. This solution was allowed to cool to ambient temperature gradually to afford **Gel2**, consisting of gelator **1** with **2a** or **2b**. Au(I) was then obtained as chloro(tetrahydrothiophene) gold(I) from HAuCl_4 precursor as described in Scheme S3. For preparation of **Gel3**, 0.5−5.0 equiv of Au(I) was added to the vial prior to mixing and heating to 30−40 °C. The mixture underwent bath sonication for 3 min to get a homogeneous solution. Gradual cooling to room temperature was carried out in the dark prior to UV light irradiation. Photoreduction of Au(I) ions was performed using a 50 mV Hg lamp (254 nm) with variable irradiation times. A quartz cell (length 80 mm, inner diameter 10 mm, and wall thickness 0.1 mm) was used in the photoreactor during reduction, and the temperature was maintained at 25 °C.

Microscopy Studies. For transmission electron microscopy (TEM), the samples of gel were placed on a carbon-coated copper grid (400 mesh) and then removed after 1 min, leaving some small patches of sample on the grid. This was examined using a JEOL JEM-2010 transmission electron microscope operating at 200 kV with an acceleration voltage of 100 kV and a 16 mm working distance.
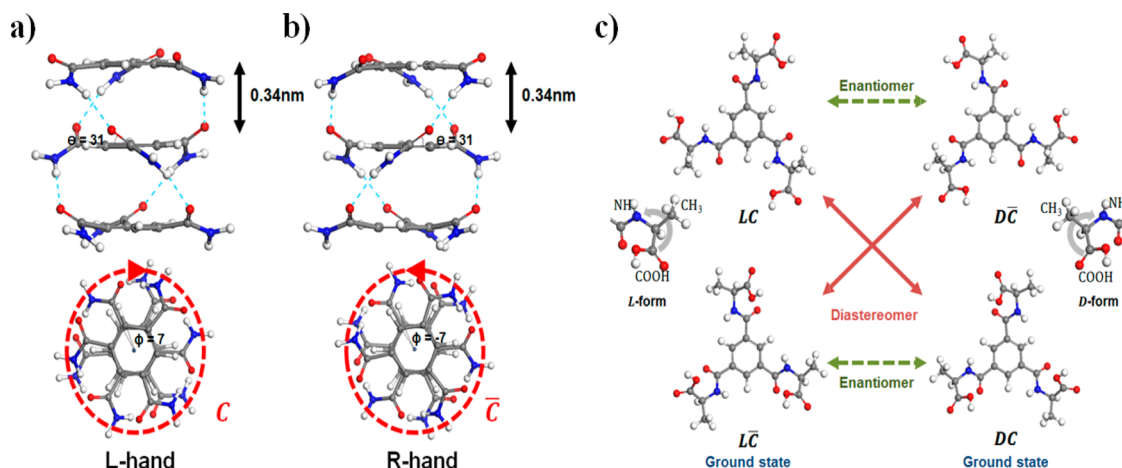
Figure 3. DFT calculation results showing: (a) interlayer hydrogen bonds of C=O dipoles aligned in a clockwise direction, C, forming a left-handed helix; (b) interlayer hydrogen bonds of C=O dipoles aligned in a counterclockwise direction, $\overline{C}$, forming a right-handed helix. C=O dipoles are twisted from the benzene plane by 31°. The upper figures are side views, showing an interlayer spacing of 0.34 nm. Hydrogen bonds are shown as cyan colored dashed lines. The lower figures are top views, showing the layer−layer tilting angle (ϕ) as ∼ ±7°. (c) Four different isomers labeled as LC, DC, $L\overline{C}$, and $D\overline{C}$ representing the chirality given two different chiral centers (i.e., the orientation of C=O dipoles denoted as C and $\overline{C}$, and the chirality of the carbon center in the side chains denoted as D and L).

Scanning electron micrographs of the samples were taken with a field emission scanning electron microscope (Philips XL30 S FEG). The acceleration voltage employed was 5−15 kV, and the emission current was 10 μA. Atomic force microscope (AFM) imaging was performed using a PPP-NCHR 10 M cantilever (Park systems). The AFM samples of gel were prepared by spin-coating (1500 rpm) onto freshly cleaved Muscovite Mica, and images were recorded with the AFM operating in tapping mode in air at RT with resolution of 1024 × 1024 pixels, using moderate scan rates (0.3 Hz).

Photophysical and CD Studies. The absorption spectra of the samples were obtained using a UV−vis spectrophotometer (Thermo Evolution 600). All fluorescence spectra were recorded with a RF-5301PC spectrophotometer. UV−vis absorption and fluorescence emission spectra (using an excitation wavelength of 282 nm) were determined over the range of 200−800 nm. Spectra were acquired for both the gel directly at room temperature and also dispersed in 1:1 DMSO/H$_2$O. UV−vis absorption spectra of **1** ([**1**] = 10 mM) were observed in the presence of **2a** or **2b** (0−2 equiv). CD spectra were recorded on a Jasco J-815 CD spectrophotometer. CD spectra were determined over the range of 230−900 nm using a quartz cell with 0.1 mm path length. Scans were taken at a rate of 100 nm/min with a sampling interval of 1.0 nm and response time of 1s. The scans were acquired for the gel directly at room temperature in 1:1 DMSO/H$_2$O. CD spectra of **1** ([**1**] = 10 mM) were observed in the presence of **2a** or **2b** (0−2 equiv) and Au(I) (0.5−5.0 equiv).

Computational Studies. DFT calculations using the M06-2X flavor coupled with the 6-311G**++ basis set were carried out using Jaguar 9.0 package [Maestro; Schrödinger, LLC: New York, 2009]. As noted, the orientation of C=O dipole moments (which is restricted either to clockwise, C, or counterclockwise, $\overline{C}$, determines the helicity) provides one chiral center, since the carbonyl groups are no longer located in the same plane as the phenyl ring. If we label the chirality of the carbon center of the side chains as "L" or "D" depending on whether L- or D-form alanine were incorporated, there exists four different isomers which can be labeled as LC, DC, $L\overline{C}$, and $D\overline{C}$ as shown in Figure 3c. It is noted that LC and DC are optical isomers to $D\overline{C}$ and $L\overline{C}$, respectively, thereby the pair LC and $D\overline{C}$ have the same energy as do the pair DC and $L\overline{C}$. However, given that two chiral centers exist, LC and DC ($L\overline{C}$ and $D\overline{C}$) are in diastereomeric relation with preferential formation of $L\overline{C}$ and DC by 0.4 kcal/mol per layer (computed from DFT calculations of one layer performed under the constraint fixing the orientation of C=O dipole twisted from the phenyl ring plane by 31°). Hence, the presence of D-form side chains (**2a**) favors clockwise alignment of C=O dipole orientations (C),

resulting in left-handed helices, while L-form side chains (**2b**) favor counterclockwise alignment of C=O dipole orientations ($\overline{C}$), resulting in right-handed helices.

RESULTS AND DISCUSSION

Initial examination of gelator **1** showed the formation of a hydrogel in which SEM and TEM images revealed nanofibers having a diameter of 20−30 nm (Figure S1). The hydrogel of gelator **1** exhibited a characteristic UV absorption peak at 282 nm (Figure 2A), and excitation at this wavelength resulted in significant fluorescence centered at 417 nm (Figure 2D). Trimesoyltri(D-alanine), **2a**, and trimesoyltri(L-alanine), **2b**, referred to here as the D- and L-form of the chiral molecules used to generate helicity in the nanofiber template, were prepared and added to gelator **1** in order to facilitate chiral fibers within the hydrogel. The hydrogel formed by gelator **1** was found to undergo a gradual reduction in absorbance at 282 nm and concomitant increase at 321 nm upon addition of D-form **2a**, as intercalation of the chiral component introduced helical arrangement of the nanofibers. Similarly, a decrease in fluorescence at 417 nm was observed as the amount of **2a** or **2b** was increased (Figures 2D and S2). The CD intensities of hydrogel **2** upon addition of 2 equiv of **2a** or **2b** were lower than those obtained for 1 equiv of **2a** or **2b**, because when 1 equiv of **2a** or **2b** is mixed with gelator **1**, all of the molecules of **2a** or **2b** are incorporated forming the nanofibers of the new hydrogel **2**. However, when 2 equiv of **2a** or **2b** are mixed with gelator **1**, then an equal proportion of **2a** or **2b** molecules will exist as a species not incorporated into the supramolecular structure (Figure S3). These free components do not contribute to the gel formation, and their presence disrupts the continuous formation of the surrounding nanofibers thereby decreasing the overall signal intensity.

As seen from the vial inversion pictures displayed in Figure 1, the material also existed as a stable hydrogel after formation of the helical nanofiber structures directed by **2a** or **2b**. In addition, observing the CD spectra of the hydrogel revealed a noticeable enhancement in the optical activity for increasing amounts of **2a** or **2b**. Comparing the CD spectra maxima at 364 nm, we could identify an optimum enhancement when

using a 1:1 mol equiv of gelator **1** to **2a** or **2b** (Figure 2B,C). The hydrogel formed by gelator **1** provided negligible contributions to the linear dichroism spectra. Furthermore, the fluorescence detected (FD) CD spectrum of hydrogel **1** with **2a** exhibited a negative sign for the first Cotton effect, whereas FDCD spectrum of hydrogel **1** with **2b** exhibited a positive sign for the first Cotton effect (Figure 2E) suggesting opposite helical handedness.

To clarify the origin of the different helical propensity depending on the chiral component used, optimized structures of individual chiral components **2a** or **2b** were assessed through DFT simulations. CD spectroscopy confirmed that the D-form (**2a**) results in left-handed helical rotations, while the L-form (**2b**) appears as right-handed stabilized helical rotations (Figure 3). The initial computations comprised a three-layer structure of phenyl rings with three $CONH_2$ side chains, since this was the common central component of the helical fibers. We find that the helical structure is driven by the formation of strong interlayer hydrogen bonds between the carbonyl group (C=O) and amine (N−H) group as shown in Figure 3, which is consistent with the experimental X-ray diffraction refined structures. We find that the direction of C=O dipoles are required to be twisted from the phenyl ring plane by ∼31° from the side view and also aligned in either a clockwise or counterclockwise pattern from the top view in order to stabilize the helical structure formation. Importantly, it is the orientation of C=O dipoles which determines the overall helicity of the entire fiber. Left-handed helices are formed by the clockwise arrangement (Figure 3a), and right-handed helices are formed by the counterclockwise arrangement of C=O dipoles (Figure 3b). The interlayer spacing computed as 0.34 nm is in excellent agreement with powder X-ray diffraction analysis of structures of gelator **1** formed in the presence and absence of D-form **2a** confirming an interplanar spacing of 0.34 nm (Figure S4). Further assessment of incorporated **2a** was revealed by IR spectroscopy (Figure S5). IR spectra were recorded for mixtures of gelator **1** and **2a**. Upon increasing the amount of **2a** in hydrogel **1**, the C=O stretching bond of gelator **1** shifts to lower wavenumbers, in agreement with the participation of hydrogen bonding in the aggregation process. NMR peaks are observed for the mobile components, while signals from immobilized components, for example within gel fibers, are effectively broadened into the baseline. Variable-temperature NMR was used to examine the temperature response of gelator **1** in the presence of **2a**. We could gain a quantitative insight into the relative amount of mobile gelator **1** and **2a** within the fibers by observing the spectra of gelator **1** with **2a** in DMSO-d_6 at increasing temperatures (Figures S6A and S6B) and referencing the integrated NMR peak associated with gelator **1** and **2a** to that associated with the mobile DMSO solvent molecules. In this analysis, we can assume that the contribution from immobile gelator **1** and **2a** is zero. As the temperature decreased, the ratio of solvent to gelator **1** or **2a** was found to increase. As a result, the NMR peaks of gelator **1** and **2a** became smaller relative to the solvent upon cooling, which is consistent with gelator **1** and **2a** becoming immobilized as sample transforms into a gel upon decreasing temperature. The largest changes in peak height, by inference of the gelator mobility, occurred around 30−60 °C, which is consistent with DSC data (Figure S6C).

Closer inspection of the computational results suggests a layer by layer tilt of ∼ ± 7° with respect to the bottom layer (+ for left-handed one, − for right-handed), leading to an overall

helical pitch of ∼17 nm. In comparison, the experimental pitch values observed from AFM measurement are 30.6 ± 8.46 nm. This is expected to arise from the lack of bulky side groups used in our simple three-layer model resulting in a shorter helical pitch and/or the usage of only three layers in our model resulting in a more twisted helix. From AFM images (Figure 4),
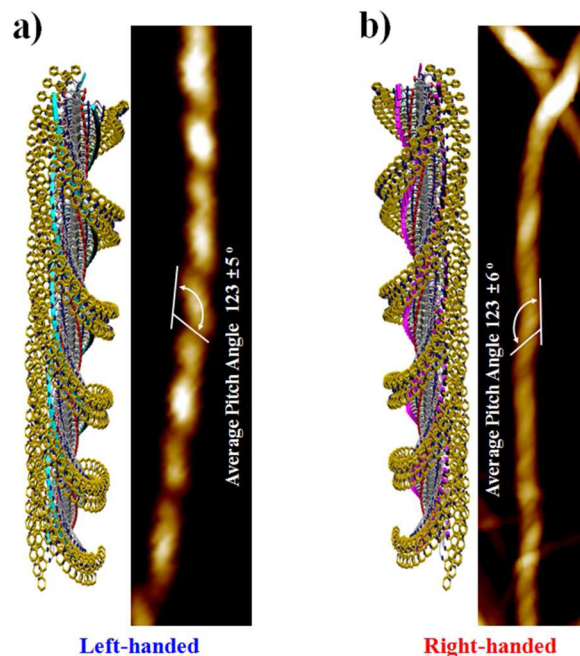

Figure 4. Model (left) and AFM images (right) of helical nanofibers comprising hydrogel **1** containing 1 equiv of (a) **2a** (D-form) or (b) **2b** (L-form).

we could determine that each nanofiber adopted a twisted helical morphology with controllable helicity (left-handed when adding the D-form **2a** or right-handed when adding the L-form **2b**). Furthermore, we determined the pitch angle of the twisted nanofibers to be 123° on average for the equimolar mixtures of gelator **1** with **2a** or **2b**.

When examining **2a** and **2b**, which possess chiral carbons in the side chains, the system is found to have two different chiral centers. From computational studies (Figure 3c), we find that the introduction of D-formed side chains energetically favors the formation of a clockwise alignment of C=O dipole orientations (C), yielding a left-handed helix, while the introduction of L-formed side chains energetically favors the formation of a counterclockwise alignment of C=O dipole orientations ($\bar{C}$), yielding a right-handed helix, which is consistent with our experimental observations (Figure S7). As our simulations and spectroscopic data suggest, the rotation of stacked chiral gelators is a result of hydrogen-bond stabilization and steric effects, thereby resulting in regular helical twisting throughout the nanofiber. Hence, utilizing different chiral components (**2a** and **2b**), we could facilitate the formation of left- or right-handed helical nanofiber-derived hydrogels.

After observing the ability of the nanofibers to serve as templates for the growth of gold nanoparticles via UV reduction of Au(I), we carried out CD spectroscopy to observe the helicity and optical activity of the resulting material before and after addition of different amounts of Au(I). After UV photoreduction of hydrogel **2** in the presence of Au(I) ions at various concentration, we observed a significant enhancement

in optical activity when using 3.0 equiv or more of Au(I) with respect to the amount of gelator **1** (Figures 5 and S8). In
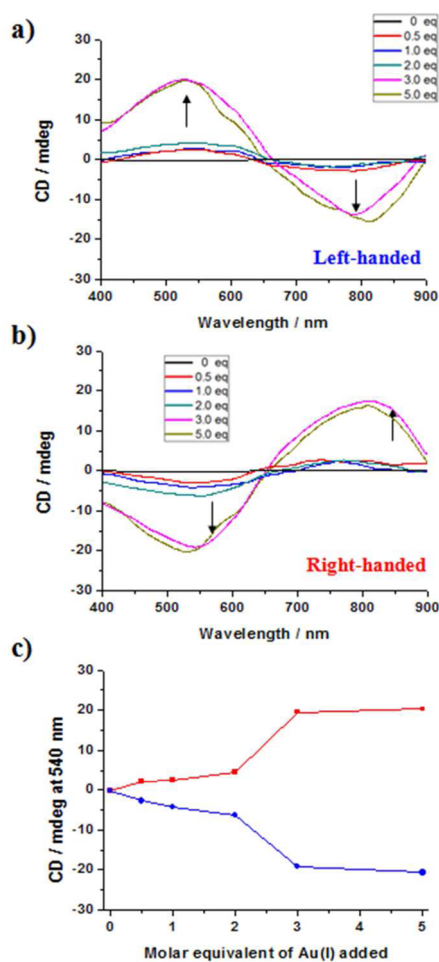

Figure 5. CD spectra after UV irradiation of hydrogel **1** containing 1 equiv of (a) **2a** or (b) **2b** in the presence of varying amounts of Au(I) ions. (c) Direct comparison of the 540 nm CD peak reveals that >3.0 mol equiv of Au(I) ion (with respect to gelator **1**) shows significant formation of gold nanoparticle superstructures.

addition, the handedness of the helical nanoparticle path, as controlled by chirality of the particular helix generating molecule, resulted in enhancement of either positive or negative CD signals. The evolution of this optical activity is attributed to the photoreductive growth of gold nanoparticles on the template nanofiber, resulting in helically coupled plasmon absorption due to the chiral arrangement of gold nanoparticles, and not from the signal of the chiral compounds **2a** and **2b**. The reduction of Au(I) ions into gold nanoparticles at the site of the chiral **2a** and **2b** templates allows such plasmon coupling throughout the helical superstructure. Further spectroscopic studies revealed that the helically coupled plasmon absorption could be changed depending on the duration of UV irradiation (Figure 6). The zero crossing of the CD spectrum reveals a shift from 560 to 658 nm providing a convenient measure of the corresponding red shift in plasmon absorption as a result of UV photoreduction induced growth of nanoparticles on the helical nanofibers as confirmed by TEM (Figures 7 and S9). It is known that increasing the size of nanoparticles within a helical arrangement can enhance the CD signal and provide a corresponding shift in the absorption peak
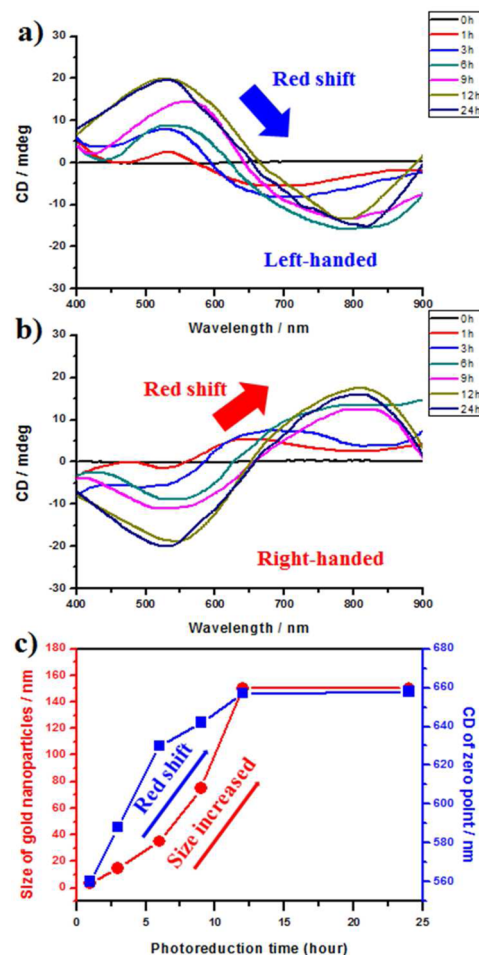

Figure 6. CD spectra of hydrogel **1** containing 1 equiv of (a) **2a** or (b) **2b** and 3 mol equiv of Au(I) ions (with respect to gelator **1**) after increasing durations of UV irradiation for reductive growth of gold nanoparticles on the helical nanofibers. (c) The zero crossing of the CD spectrum reveals a shift from 560 to 658 nm as a result of UV photoreduction induced growth of nanoparticles on the helical nanofibers confirmed by the corresponding red shift in plasmon absorption.

to longer wavelengths.[5a,16] With this in mind, our template-based system can provide controlled growth of helically arranged gold nanoparticles to offer CD active materials with distinct, tunable absorption properties throughout a range of the visible spectrum via the coupled plasmon frequency. This is in agreement with our TEM analysis revealing high-quality superstructures containing well-defined helicity of increasingly sized gold nanoparticle arrangements as can be observed in Figure 6. To confirm the presence of gold nanoparticles deposited on the helical nanofiber gel, the fibers were observed by energy dispersive X-ray spectroscopy (EDX) coupled with TEM measurements (Figure S10). Elemental mapping by EDX with TEM shows the gel fiber consists of carbon (C), oxygen (O), nitrogen (N), and gold (Au) components and further indicates that the gold nanoparticles are deposited on the gel fiber.

■ CONCLUSIONS

In summary, our approach to chiroptical materials development may help to extend the length scales of organized gold nanoparticles on helical nanofibers up to hundreds of
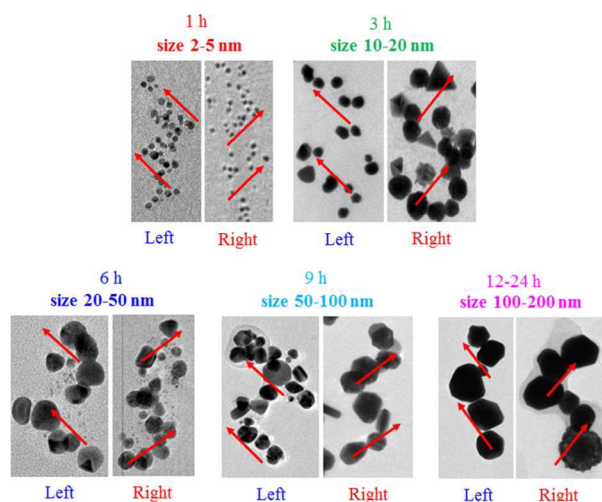
6451

dx.doi.org/10.1021/ja5018199 | *J. Am. Chem. Soc.* 2014, 136, 6446−6452

Figure 7. TEM images of nanoparticle superstructures from hydrogel **1** containing 1 equiv of **2a** (D-form) or 1 equiv of **2b** (L-form) for various durations of UV irradiation to control the size of gold nanoparticles grown on the helical nanofiber template.

nanometers in length with tunable nanoparticles diameters ranging from 2 nm up to 200 nm. The size of the gold nanoparticles comprising the superstructures could be easily controlled by UV irradiation time to facilitate flexibility in terms of the desired plasmon absorption wavelength. Moreover, we provide the first modular system in which the chiroptical properties of the hydrogels can be easily customized by addition of D- or L-form helical introducing molecules to yield materials exhibiting a positive first Cotton effect and negative first Cotton effect, respectively. Utilizing this modular template in combination with controlled nanoparticle growth can offer high yield, "bottom-up" assembly which we expect to be of significant value to researchers requiring materials with customizable chiroptical properties.

■ ASSOCIATED CONTENT

Ⓢ Supporting Information

Experimental details and characterization data.This material is available free of charge via the Internet at http://pubs.acs.org.

■ AUTHOR INFORMATION

Corresponding Authors
linus16@kaist.ac.kr
justynj@hanyang.ac.kr
jonghwa@gnu.ac.kr

Notes
The authors declare no competing financial interest.

■ ACKNOWLEDGMENTS

■ REFERENCES

(1) (a) Nie, Z.; Petukhova, A.; Kumacheva, E. *Nat. Nanotechnol.* **2010**, *5*, 15. (b) Shenhar, R.; Norsten, T. B.; Rotello, V. M. *Adv. Mater.* **2005**, *17*, 657. (c) Grzelczak, M.; Vermant, J.; Furst, E. M.; Liz-Marzán, L. M. *ACS Nano* **2010**, *4*, 3591.

(2) (a) Kaminker, R.; Lahav, M.; Motiei, L.; Vartanian, M.; Popovitz-Biro, R.; Iron, M. A.; van der Boom, M. E. *Angew. Chem., Int. Ed.* **2010**, *49*, 1218. (b) Chen, W.; Bian, A.; Agarwal, A.; Liu, L.; Shen, H.; Wang, L.; Xu, C.; Kotov, N. A. *Nano Lett.* **2009**, *9*, 2153.

(3) (a) Mirkin, C. A.; Letsinger, R. L.; Mucic, R. C.; Storhoff, J. J. *Nature* **1996**, *382*, 607. (b) Alivisatos, A. P.; Johnsson, K. P.; Peng, X.; Wilson, T. E.; Loweth, C. J.; Bruchez, M. P.; Schultz, P. G. *Nature* **1996**, *382*, 609. (c) Martin, C. P.; Blunt, M. O.; Pauliac-Vaujour, E.; Stannard, A.; Moriarty, P.; Vancea, I.; Thiele, U. *Phys. Rev. Lett.* **2007**, *99*, 116103.

(4) (a) Kuzyk, A.; Schreiber, R.; Fan, Z.; Pardatscher, G.; Roller, E.-M.; Hogele, A.; Simmel, F. C.; Govorov, A. O.; Liedl, T. *Nature* **2012**, *483*, 311. (b) Pandoli, O.; Massi, A.; Cavazzini, A.; Spada, G. P.; Cui, D. *Analyst* **2011**, *136*, 3713. (c) Sharma, J.; Chhabra, R.; Cheng, A.; Brownell, J.; Liu, Y.; Yan, H. *Science* **2009**, *323*, 112.

(5) (a) Chen, C.-L.; Zhang, P.; Rosi, N. L. *J. Am. Chem. Soc.* **2008**, *130*, 13555. (b) Slocik, J. M.; Govorov, A. O.; Naik, R. R. *Nano Lett.* **2011**, *11*, 701. (c) Slocik, J. M.; Tam, F.; Halas, N. J.; Naik, R. R. *Nano Lett.* **2007**, *7*, 1054.

(6) Meister, A.; Drescher, S.; Mey, I.; Wahab, M.; Graf, G.; Garamus, V. M.; Hause, G.; Mogel, H.-J.; Janshoff, A.; Dobner, B.; Blume, A. *J. Phys. Chem. B* **2008**, *112*, 4506.

(7) (a) Li, Z.; Zhu, Z.; Liu, W.; Zhou, Y.; Han, B.; Gao, Y.; Tang, Z. *J. Am. Chem. Soc.* **2012**, *134*, 3322. (b) Guerrero-Martínez, A.; Auguié, B.; Alonso-Gómez, J. L.; Džolić, Z.; Gómez-Graña, S.; Žinić, M.; Cid, M. M.; Liz-Marzán, L. M. *Angew. Chem., Int. Ed.* **2011**, *50*, 5499. (c) Wang, R.-Y.; Wang, H.; Wu, X.; Ji, Y.; Wang, P.; Qu, Y.; Chung, T.-S. *Soft Matter* **2011**, *7*, 8370.

(8) Shemer, G.; Krichevski, O.; Markovich, G.; Molotsky, T.; Lubitz, I.; Kotlyar, A. B. *J. Am. Chem. Soc.* **2006**, *128*, 11006.

(9) Chen, C.-L.; Rosi, N. L. *J. Am. Chem. Soc.* **2010**, *132*, 6902.

(10) (a) Qi, H.; Shopsowitz, K. E.; Hamad, W. Y.; MacLachlan, M. J. *J. Am. Chem. Soc.* **2011**, *133*, 3728. (b) Xie, J.; Duan, Y.; Che, S. *Adv. Funct. Mater.* **2012**, *22*, 3784.

(11) Zhu, L.; Li, X.; Wu, S.; Nguyen, K. T.; Yan, H.; Ågren, H.; Zhao, Y. *J. Am. Chem. Soc.* **2013**, *135*, 9174.

(12) Ben-Moshe, A.; Maoz, B. M.; Govorov, A. O.; Markovich, G. *Chem. Soc. Rev.* **2013**, *42*, 7028.

(13) Kotova, O.; Daly, R.; dos Santos, C. M. G.; Boese, M.; Kruger, P. E.; Boland, J. J.; Gunnlaugsson, T. *Angew. Chem., Int. Ed.* **2012**, *51*, 7208.

(14) Chen, Z.; Liu, X.; Zhang, C.; Zhang, Z.; Liang, F. *Dalton Trans.* **2011**, *40*, 1911.

(15) Uson, R.; Laguna, A.; Laguna, M.; Briggs, D. A.; Murray, H. H.; Fackler, J. P. (Tetrahydrothiophene) gold(I) or gold(III) complexes. In: *Inorganic Syntheses*; John Wiley & Sons, Inc.: Hoboken, NJ, 2007.

(16) Fan, Z.; Govorov, A. O. *Nano Lett.* **2010**, *10*, 2580.